JACS ARTICLES

Published on Web 05/27/2010

# Crystal Growth and Structure and Magnetic Properties of the 5d Oxide $Ca_3LiOsO_6$: Extended Superexchange Magnetic Interaction in Oxide

Youguo Shi,[†,‡] Yanfeng Guo,[†,‡] Shan Yu,[‡,§] Masao Arai,[||] Akira Sato,[⊥] Alexei A. Belik,[†,‡] Kazunari Yamaura,[*,‡,§,#] and Eiji Takayama-Muromachi[†,‡,§,#]

*International Center for Materials Nanoarchitectonics, Superconducting Materials Center, Computational Materials Science Center, and Materials Analysis Station, National Institute for Materials Science, 1-1 Namiki, Tsukuba, Ibaraki 305-0044, Japan, Transformative Research-Project on Iron Pnictides (TRIP), JST, 5 Sanbancho, Chiyoda-ku, Tokyo 102-0075, Japan, and Department of Chemistry, Graduate School of Science, Hokkaido University, Sapporo, Hokkaido 060-0810, Japan*

Received March 29, 2010; E-mail: yamaura.kazunari@nims.go.jp

***Abstract:*** Crystals of the newly synthesized compound $Ca_3LiOsO_6$ were grown by a flux method using LiCl and KCl, followed by single-crystal X-ray diffraction (XRD), low-temperature powder XRD, and measurements of ac and dc magnetic susceptibility and specific heat. The data indicate that $Ca_3LiOsO_6$ has a fully opened electronic gap with an antiferromagnetic ordered state, consistent with suggestions from the first-principles study. The observed magnetic transition temperature is 117 K, too high to be caused only by a direct spin−spin interaction. It appears that the original superexchange magnetic path Os−O−Os is absent; thus, the extended superexchange path (Os−O)−(O−Os) can be expected to be responsible for the 117 K magnetic order. If this is true, $Ca_3LiOsO_6$ would be highly valuable to study the nature of extended superexchange magnetic interactions in solids.

## 1. Introduction

Superexchange magnetic interaction was first proposed by Kramers in the 1930s[1] and refined by Anderson[2] in 1950. The magnetic interaction model was further developed by Goodenough and others.[3] The model is often called the "Goodenough−Kanamori rule", and it is useful to predict features of a magnetic interaction between two next-nearest-neighbor cations through a nonmagnetic anion not only qualitatively but also quantitatively. For example, the magnetic properties of the perovskite-based transition metal (Tr) oxide are well-characterized by the model.[3] A model of the magnetic interaction through multiple oxygen atoms (extended superexchange interaction) seems, however, is not as well-developed, although leading experimental and theoretical studies were conducted to some extent on several 3d oxides, including Cu−O chain compounds, $(VO)_2P_2O_7$, $VO(HPO_4)\cdot 0.5H_2O$, and $Cu_2Te_2O_5X_2$ (X = Cl, Br).[4−7] The 3d oxides contain not only the extended superexchange interaction but also the original superexchange interaction (M−O−M); thus, analysis of the magnetism and the interactions is often complicated. A magnetic system solely comprising a magnetic path through multiple oxygen atoms is therefore highly expected to promote understanding of the nature of the extended superexchange interaction in oxides.

In our studies of several osmium oxides, including $NaOsO_3$ (a possible room-temperature Slater insulator)[8] and $Na_2OsO_4$,[9] we obtained a crystal having the composition $Ca_3LiOsO_6$, probably for the first time. The crystal structure was successfully identified by single-crystal X-ray diffraction (XRD) to be of the $K_4CdCl_6$ type.[10] Afterward, we learned that $K_4CdCl_6$-type oxides form a large family (the general formula is often written as $A_3A'MO_6$),[11] and many of them show unusual magnetic properties, such as a random ferromagnetic (FM) and antiferromagnetic (AF) interplay between quantum effects and disorder

[†] International Center for Materials Nanoarchitectonics, National Institute for Materials Science.
[‡] TRIP, JST.
[§] Superconducting Materials Center, National Institute for Materials Science.
[||] Computational Materials Science Center, National Institute for Materials Science.
[⊥] Materials Analysis Station, National Institute for Materials Science.
[#] Hokkaido University.

(1) Kramers, H. A. *Physica* **1934**, *1*, 182.
(2) Anderson, P. W. *Phys. Rev.* **1950**, *79*, 350.
(3) Goodenough, J. B. *Magnetism and the Chemical Bond*; Interscience-Wiley: New York, 1963.
(4) Mizuno, Y.; Tohyama, T.; Maekawa, S. *Phys. Rev. B* **1999**, *60*, 6230.
(5) Mizuno, Y.; Tohyama, T.; Maekawa, S. *Phys. Rev. B* **1998**, *58*, R14713.
(6) Mizuno, Y.; Tohyama, T.; Maekawa, S.; Osafune, T.; Motoyama, N.; Eisaki, H.; Uchida, S. *Phys. Rev. B* **1998**, *57*, 5326.
(7) Whangbo, M.-H.; Koo, H.-J.; Dai, D. *J. Solid State Chem.* **2003**, *176*, 417.
(8) Shi, Y. G.; Guo, Y. F.; Yu, S.; Arai, M.; Belik, A. A.; Sato, A.; Yamaura, K.; Takayama-Muromachi, E.; Tian, H. F.; Yang, H. X.; Li, J. Q.; Varga, T.; Mitchell, J. F.; Okamoto, S. *Phys. Rev. B* **2009**, *80*, 161104(R).
(9) Shi, Y. G.; Guo, Y. F.; Yu, S.; Arai, M.; Belik, A. A.; Sato, A.; Yamaura, K.; Takayama-Muromachi, E.; Varga, T.; Mitchell, J. F. *J. Solid State Chem.* **2010**, *183*, 402.
(10) Bergerhoff, G.; Schmitz-Dumont, O. *Z. Anorg. Allg. Chem.* **1956**, *284*, 10.
(11) Stitzer, K. E.; Darriet, J.; zur Loye, H.-C. *Curr. Opin. Solid State Mater. Sci.* **2001**, *5*, 535.

 **10.1021/ja102606q** 

in $Sr_3Cu(Pt,Ir)O_6$,[12−14] and magnetic frustration in a partially disordered antiferromagnetic (PDA) state in $Ca_3Co_2O_6$ ($T_N$ = 25 K)[15−19] and $Ca_3CoIrO_6$ ($T_N$ = 30 K).[20] Hence, we focused on the magnetic properties of the newly synthesized compound $Ca_3LiOsO_6$.

At the beginning, we looked at the magnetic properties of the family, including $Sr_3LnNiO_6$ (Ln = Sc, In, Tm, Yb, and Lu; no magnetic order above 6 K),[21] $Sr_3PbNiO_6$ ($T_N$ = 6 K),[22] $Sr_3LnCrO_6$ (Ln = Sc, In, Lu, Yb, Tm, Er, Ho, and Y; the highest $T_N$ of the series is ∼15 K),[23,24] $Sr_3NiRhO_6$ ($T_1$ = 45 K and $T_2$ = 10 K in a PDA state),[25] $Sr_3MgRhO_6$ ($T_N$ = 13 K),[26] $Sr_3CaRhO_6$ ($T_N$ = 7 K),[27] $Sr_3LnRhO_6$ (Ln = Y, Sc, In, Sm, Eu, Er, Tb, Yb, Ho, and Dy; no magnetic order above 5 K),[28,29] $Sr_4RhO_6$ ($T_N$ = 7 K),[30] $Ca_3CoRhO_6$ ($T_1$ = 90 K and $T_2$ = 30 K in a PDA state),[31] $Ca_3CuRhO_6$ ($T_N$ = 15 K),[32] $Sr_3LiRhO_6$ and $Sr_3NaRhO_6$ (no magnetic order above 5 K),[33] $Sr_3LiRuO_6$ ($T_N$ = 90 K),[34] $Sr_3NaRuO_6$ ($T_N$ = 70 K),[34] $Ca_3NaRuO_6$ ($T_N$ = 90 K),[34,35] $Ca_3LiRuO_6$ ($T_N$ = 120 K),[34] $Sr_3ZnIrO_6$ (no magnetic order above 10 K),[36] $Sr_3CuIrO_6$ ($T_C$ = 40 K),[37] $Sr_3NiIrO_6$ (a singlet ground state below 15 K),[37] $Sr_4IrO_6$ ($T_N$ = 12 K),[38,39] $Sr_3MgIrO_6$ ($T_N$ = 13 K),[40] $Sr_3CdIrO_6$ ($T_N$ = 22 K),[41] $Sr_3CaIrO_6$ ($T_N$ = 14 K),[41] $Ca_3CuIrO_6$ ($T_N$ = 15 K),[32] $Ca_4IrO_6$ ($T_N$ = 16 K),[41] $Ca_{4-x}Ni_xIrO_6$ (the highest $T_N$ of the series is ∼13 K),[42] $Ca_3NaIrO_6$ (magnetic properties were unreported),[43] $Ca_3MgIrO_6$ and $Ca_3ZnIrO_6$ (magnetic properties were unreported),[44] $Sr_3ZnPtO_6$ (nonmagnetic),[45] $Sr_3NiPtO_6$ (no magnetic order above 1.8 K),[25,46] $Sr_3CoPtO_6$ ($T_N$ = 1.4 K),[45] and $Sr_4PtO_6$ (nonmagnetic).[47] The above compounds are listed in the order of M = 3d, 4d, and 5d atoms. Several non-d-electron members were also studied as well, such as $Ba_3NaMO_6$ (M = Nb,[48] Ta,[48] Bi[49]), $Sr_3NaMO_6$ (M = Nb,[50] Ta,[50] Bi,[49] Sb[51]), and $Sr_3LiBiO_6$.[49]

Throughout the survey, we found that $Sr_3LiRuO_6$, $Sr_3NaRuO_6$, $Ca_3NaRuO_6$, and $Ca_3LiRuO_6$ are outstanding with regard to the magnetic transition temperature: they evidently show an AF transition between 70 and 120 K, remarkably high for this family. Here we present a generalized image of the crystal structure of the family:[11] The $K_4CdCl_6$-type oxide consists of infinite magnetic chains in a triangular arrangement. Each chain consists of octahedral $MO_6$ and trigonal prism $A'O_6$, which are connected by sharing their polyhedral faces. The infinite magnetic chains are separated well by A atoms; thus, the complex magnetic properties often include low-dimensional magnetism, geometrical frustration, and alternate-chain magnetism of $MO_6$ and $A'O_6$. Nevertheless, the Ru oxides $A_3A'RuO_6$ (A = Sr and Ca; A′ = Li and Na) show a conventional long-range AF order (some show a weak ferromagnetism, but the AF order is intrinsic) at unusually high temperature without remarkable low-dimensional magnetism, geometrical frustration, and alternate-chain magnetism. The $T_N$ of 120 K reported for $Ca_3LiRuO_6$ is the highest recorded for the family. The three-dimensional (3D) AF order was confirmed by a neutron-diffraction study.[34] It is apparent that $A_3A'RuO_6$ is far different from other members, regarding the nature of the magnetism; however, the origin of the exceptional magnetism remains unrevealed.[34]

In this study, we found that the newly synthesized $Ca_3LiOsO_6$ shows an analogous AF transition at 117 K, implying that the AF order is not due to the nature of Ru but likely is due to the common electronic configuration $t_{2g}^3$ ($S$ = 3/2), regardless of 4d and 5d. Based on studies of $Ca_3LiTrO_6$ (Tr = Ru and Os), it is most likely that the extended superexchange interaction is responsible for the 117 K AF order. If this is true, $Ca_3LiOsO_6$ as well as $Ca_3LiRuO_6$ can be valuable for further studies of the extended superexchange interaction in solids.

## 2. Experimental Section

Single crystals of $Ca_3LiOsO_6$ were grown through two major steps. The first step was to prepare polycrystalline $Ca_3OsO_6$.[52] We started the synthesis with the preparation of $CaO_2$ powder: $CaCl_2$


(12) Irons, S. H.; Sangrey, T. D.; Beauchamp, K. M.; Smith, M. D.; zur Loye, H.-C. *Phys. Rev. B* **2000**, *61*, 11594.
(13) Nguyen, T. N.; Lee, P. A.; zur Loye, H.-C. *Science* **1996**, *271*, 489.
(14) Furusaki, A.; Sigrist, M.; Lee, P. A.; Tanaka, K.; Nagaosa, N. *Phys. Rev. Lett.* **1994**, *73*, 2622.
(15) Cheng, J.-G.; Zhou, J.-S.; Goodenough, J. B. *Phys. Rev. B* **2009**, *79*, 184414.
(16) Agrestini, S.; Chapon, L. C.; Daoud-Aladine, A.; Schefer, J.; Gukasov, A.; Mazzoli, C.; Lees, M. R.; Petrenko, O. A. *Phys. Rev. Lett.* **2008**, *101*, 097207.
(17) Kudasov, Y. B. *Phys. Rev. Lett.* **2006**, *96*, 027212.
(18) Wu, H.; Haverkort, M. W.; Hu, Z.; Khomskii, D. I.; Tjeng, L. H. *Phys. Rev. Lett.* **2005**, *95*, 186401.
(19) Burnus, T.; Hu, Z.; Haverkort, M. W.; Cezar, J. C.; Flahaut, D.; Hardy, V.; Maignan, A.; Brookes, N. B.; Tanaka, A.; Hsieh, H. H.; Lin, H.-J.; Chen, C. T.; Tjeng, L. H. *Phys. Rev. B* **2006**, *74*, 245111.
(20) Rayaprol, S.; Sengupta, K.; Sampathkumaran, E. V. *Phys. Rev. B* **2003**, *67*, 180404(R).
(21) James, M.; Attfield, J. P. *Chem.—Eur. J.* **1996**, *2*, 737.
(22) Smith, M. D.; Stalick, J. K.; zur Loye, H.-C. *Chem. Mater.* **1999**, *11*, 2984.
(23) Smith, M. D.; Stalick, J. K.; zur Loye, H.-C. *Chem. Mater.* **2000**, *12*, 2404.
(24) Hardy, V.; Martin, C.; Martinet, G. *Phys. Rev. B* **2006**, *74*, 064413.
(25) Mohapatra, N.; Iyer, K. K.; Rayaprol, S.; Sampathkumaran, E. V. *Phys. Rev. B* **2007**, *75*, 214422.
(26) Nunez, P.; Trail, S.; zur Loye, H.-C. *J. Solid State Chem.* **1997**, *130*, 35.
(27) Vente, J. F.; Lear, J. K.; Battle, P. D. *J. Mater. Chem.* **1995**, *5*, 1785.
(28) Layland, R. C.; Kirkland, S. L.; Nunez, P.; zur Loye, H.-C. *J. Solid State Chem.* **1998**, *139*, 416.
(29) Layland, R. C.; Kirkland, S. L.; zur Loye, H.-C. *J. Solid State Chem.* **1998**, *139*, 79.
(30) Vente, J. F.; Lear, J. K.; Battle, P. D. *J. Mater. Chem.* **1995**, *5*, 1785.
(31) Niitaka, S.; Yoshimura, K.; Kosuge, K.; Nishi, M.; Kakurai, K. *Phys. Rev. Lett.* **2001**, *87*, 177202.
(32) Rayaprol, S.; Sampathkumaran, E. V. *Phys. Rev. B* **2005**, *71*, 094403.
(33) Reisner, B. A.; Stacy, A. M. *J. Am. Chem. Soc.* **1998**, *120*, 9682.
(34) Darriet, J.; Grasset, F.; Battle, P. D. *Mater. Res. Bull.* **1997**, *32*, 139.
(35) Claridge, J. B.; Layland, R. C.; Adams, R. D.; zur Loye, H.-C. *Z. Anorg. Allg. Chem.* **1997**, *623*, 1131.
(36) Lampe-Onnerud, C.; Sigrist, M.; zur Loye, H.-C. *J. Solid State Chem.* **1996**, *127*, 25.
(37) Nguyen, T. N.; zur Loye, H.-C. *J. Solid State Chem.* **1995**, *117*, 300.
(38) Powell, A. V.; Battle, P. D.; Gore, J. G. *Acta Crystallogr. C* **1993**, *49*, 852.
(39) Powell, A. V.; Gore, J. G.; Battle, P. D. *J. Alloys Compd.* **1993**, *201*, 73.
(40) Nunez, P.; Trail, S.; zur Loye, H.-C. *J. Solid State Chem.* **1997**, *130*, 35.
(41) Segal, N.; Vente, J. F.; Bush, T. S.; Battle, P. D. *J. Mater. Chem.* **1996**, *6*, 395.
(42) Layland, R. C.; zur Loye, H.-C. *Mater. Res. Bull.* **2001**, *36*, 2701.
(43) Claridge, J. B.; Layland, R. C.; Adams, R. D.; zur Loye, H.-C. *Z. Anorg. Allg. Chem.* **1997**, *623*, 1131.
(44) Davis, M. J.; Smith, M. D.; zur Loye, H.-C. *Acta Crystallogr. C* **2001**, *57*, 1234.
(45) Nguyen, T. N.; zur Loye, H.-C. In *Neutron Scattering and Materials Science*; MRS Symposium Proceedings *376*; Neumann, D. A., Russel, T. P., Wuensch, B. J., Eds.; Materials Research Society: Pittsburgh, PA, 1995; p 603.
(46) Nguyen, T. N.; Giaquinta, D. M.; zur Loye, H.-C. *Chem. Mater.* **1994**, *6*, 1642.
(47) Randall, J. J., Jr.; Katz, L. *Acta Crystallogr.* **1959**, *12*, 519.
(48) Wehrum, G.; Hoppe, R. *Z. Anorg. Allg. Chem.* **1992**, *617*, 45.
(49) Carlson, V. A.; Stacy, A. M. *J. Solid State Chem.* **1992**, *96*, 332.
(50) Bharathy, M.; Rassolov, V. A.; zur Loye, H.-C. *Chem. Mater.* **2008**, *20*, 2268.
(51) Battle, P. D.; Hartwell, S. J.; Moore, C. A. *Inorg. Chem.* **1996**, *6*, 395.
(52) Chamberland, B. L. *Mater. Res. Bull.* **1978**, *13*, 1273.

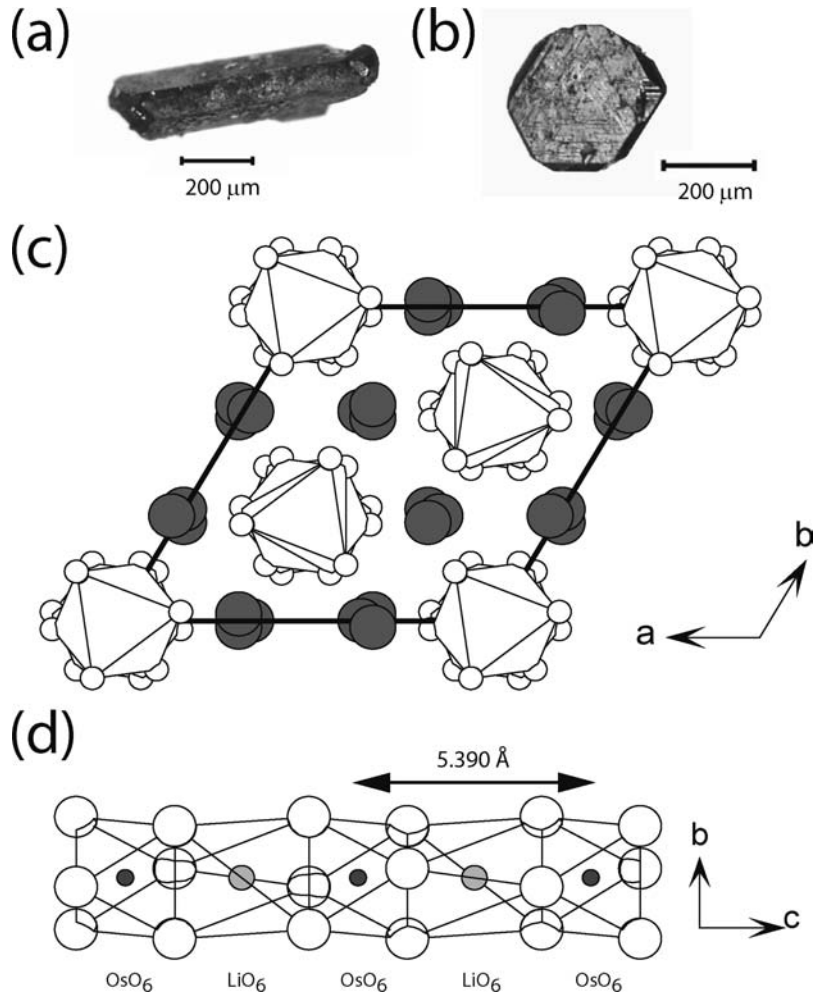


***Figure 1.*** (a,b) Photographs of flux-grown single crystals of $Ca_3LiOsO_6$. (c) The crystal structure of $Ca_3LiOsO_6$ viewed along the *c*-axis: gray spheres, Ca atoms; small spheres, O atoms; polyhedra, $LiO_6$ trigonal prisms or $OsO_6$ octahedra; solid lines, the trigonal unit cell. (d) Alternating array of $LiO_6$ trigonal prisms and $OsO_6$ octahedra in the chain: solid spheres, Os atoms; gray spheres, Li atoms; open spheres, O atoms.

(High Purity Chemicals, 99.9+%) was dissolved in 300 mL of water, followed by dropwise addition of ammonia solution and $H_2O_2$ solution. The precipitate was filtered and washed with water, followed by drying in oxygen, giving a white powder. Next, stoichiometric amounts of $CaO_2$ and Os (Koch Chemicals, 99.999%) were thoroughly mixed in an Ar-filled glovebox, and the mixture was placed in a Pt capsule. The capsule was heated in a belt-type pressure apparatus for 1 h. The elevated pressure and temperature were 6 GPa and 1500 °C, respectively. The capsule was then cooled to room temperature before releasing the pressure. The quality of the product was studied by a powder XRD method using Cu Kα radiation in a commercial apparatus (RINT 2200V, Rigaku), confirming the absence of major impurities.

The second step was to grow crystals of $Ca_3LiOsO_6$. Powders of $Ca_3OsO_6$, LiCl (Sigma-Aldrich, 99.99+ %), and KCl (Rare Metallic, 99.9%) were mixed at an approximate mass ratio of 1:5:2 in a glovebox. The mixture was placed in a Pt crucible, sealed in an evacuated silica tube, and heated at 750 °C for 12 h. The final product was immersed in water for 3 h and washed well with fresh water for a few minutes. The crystals grew as shiny hexagonal black rods or platelets, as shown in Figure 1a,b. Subsequently, polycrystalline $Ca_3LiOsO_6$ was synthesized by means of a solid-state reaction from CaO (lab-made),[53] Os, $Li_2O$ (Aldrich, 97%), and $KClO_4$ (Kishida Chemical, 99.5%). The stoichiometric mixture was placed in a Pt crucible and sealed in an evacuated quartz tube, followed by heating at 700 °C for 20 h. The polycrystalline $Ca_3LiOsO_6$ was subjected to a low-temperature XRD study. It should be stated that the above steps were initially designed to grow crystals of $Ca_3OsO_6$ using LiCl and KCl flux; however, the crystals obtained were actually not what we intended to grow. The possibility of growing crystals of $Ca_3LiOsO_6$ under pressure was thus uninvestigated.

The crystal structure of $Ca_3LiOsO_6$ was determined by a single-crystal XRD method at ambient temperature and pressure. A crystal of $Ca_3LiOsO_6$ was mounted on the end of a fine glass fiber in a diffractometer equipped with an area detector (SMART APEX, Bruker). Monochromatic Mo Kα ($\lambda = 0.71073$ Å) radiation was used. The analysis conditions used are shown in Table 1. The software SMART and SAINT+ were employed for data acquisition and extraction/reduction, respectively.[54] An empirical absorption correction was accomplished by using the software SADABS.[54] Structure parameters were refined by a full-matrix least-squares method on the $F^2$ data using SHELXL-97.[55] The oxygen content of the crystal was not measured by a chemical method to avoid possible production of the highly toxic $OsO_4$. Throughout the present study, we assume that the oxygen component is stoichio-

(53) Yamaura, K.; Shirako, Y.; Kojitani, H.; Arai, M.; Young, D. P.; Akaogi, M.; Nakashima, M.; Katsumata, T.; Inaguma, Y.; Takayama-Muromachi, E. *J. Am. Chem. Soc.* **2009**, *31*, 2722.

(54) *SMART, SAINT+, and SADABS Packages*; Bruker Analytical X-ray Systems Inc.: Madison, WI, 2002.

(55) Sheldrick, G. M. *SHELXL-97, Program for the Solution and Refinement of Crystal Structures*; University of Göttingen: Göttingen, Germany, 1997.

***Table 1.*** Crystallographic Data and Structure Refinement for $Ca_3LiOsO_6$

| | |
|---|---|
| empirical formula | $Ca_3LiOsO_6$ |
| formula weight | 413.38 g/mol |
| temperature | 290 K |
| radiation | Mo Kα (0.71073 Å) |
| crystal system | trigonal |
| space group | *R*3*c* (No. 167) |
| unit cell dimensions | $a = 9.2738(2)$ Å |
| | $c = 10.7801(4)$ Å |
| cell volume | 802.91(4) Å$^3$ |
| *Z* | 6 |
| density, calculated | 5.129 g/cm$^3$ |
| crystal size (mm) | 0.16 × 0.10 × 0.10 |
| *h k l* range | $-16 \le h \le 16$, $-13 \le k \le 16$, $-19 \le l \le 19$ |
| $2\theta_{max}$ | 80.92 |
| linear absorption coeff. | 26.65 mm$^{-1}$ |
| absorption correction | multiscan (SADABS, Bruker, 1999) |
| $T_{min}/T_{max}$ | 0.0280/0.1180 |
| no. of reflections | 5940 |
| $R_{int}$ | 0.0459 |
| no. independent reflections | 569 |
| no. observed reflections | 557 [$F_o > 4\sigma(F_o)$] |
| *F*(000) | 1122 |
| *R* factors [a] | 2.18% ($R_1[F_o > 4\sigma(F_o)]$), 5.90% ($wR_2$) |
| weighting scheme | $w = 1/[\sigma^2(F_o^2) + (0.0307P)^2 + 3.67P]$, where $P = (\mathrm{Max}(F_o^2) + 2F_c^2)/3$ |
| diff. Fourier residues | [−2.08, 4.93] e/Å$^3$ |
| refinement software | SHELXL-97 |

[a] The more than double difference in the *R* factors is probably due to the weighting scheme used in the analysis. The large difference was observed also in the analysis of an analogous compound.[44]

***Table 2.*** Structure Parameters and Anisotropic Displacement Parameters (Å$^2$) of $Ca_3LiOsO_6$

| site | Wyckoff position | *x* | *y* | *z* | $U_{eq}$ |
|---|---|---|---|---|---|
| Os | 6*b* | 0 | 0 | 0 | 0.0079(1) |
| Ca | 18*e* | 0.64570(6) | 0 | 0.25 | 0.0107(2) |
| O | 36*f* | 0.0277(2) | 0.8442(2) | 0.39427(16) | 0.0128(3) |
| Li | 6*a* | 0 | 0 | 0.25 | 0.025(4) |

| atom | $U_{11}$ | $U_{22}$ | $U_{33}$ | $U_{12}$ | $U_{13}$ | $U_{23}$ |
|---|---|---|---|---|---|---|
| Os | 0.00836(10) | 0.00836(10) | 0.00704(12) | 0.00418(5) | 0.00000 | 0.00000 |
| Ca | 0.01129(17) | 0.0110(2) | 0.0096(2) | 0.00551(11) | −0.00043(7) | −0.00087(15) |
| O | 0.0162(6) | 0.0120(6) | 0.0114(6) | 0.0080(5) | 0.0001(5) | −0.0025(5) |
| Li | 0.028(7) | 0.028(7) | 0.019(9) | 0.014(3) | 0.00000 | 0.00000 |

metric. As a reference, several $K_4CdCl_6$-type oxides were investigated by neutron diffraction and thermogravimetric methods, and the oxygen nonstoichiometry was found to be fairly little.[22,34]

The thermal evolution of the unit cell of $Ca_3LiOsO_6$ was studied by powder XRD between 30 and 300 K in a commercial XRD instrument (M03XHF22, Mac Science). The polycrystalline powder sample and a nearly equal amount of Si powder (NIST standard 640c) were mixed well, and the mixture was spread on a thin coat of grease (Apiezon N) on a thin glass sheet. The glass was mounted on a cold stage of the instrument. Monochromatic radiation (Cu Kα) was used in the $2\theta$ range between 16 and 82°. At every temperature point, $2\theta$ was calibrated by using tabulated data of the thermal expansivity of Si.[56]

The dc magnetic susceptibility ($\chi$) of an amount of crystals (21.0 mg) was measured in a commercial instrument (Quantum Design MPMS) between 2 and 350 K in applied fields of 0.1, 1, and 10 kOe. The crystals were loosely gathered in a sample holder and cooled to the low-temperature limit. The magnetic field was then applied to the crystals, and the crystals were slowly warmed to 350 K (zero-field cooling, ZFC), followed by cooling in the field (field cooling, FC). Isothermal magnetization was measured in the instrument at 5, 115, and 300 K between −10 and 10 kOe. In order to study the crystal direction dependence of $\chi$, a single crystal (0.252 mg, measured in a microbalance) was studied as well.

The ac magnetic susceptibility ($= \chi' - i\chi''$) of $Ca_3LiOsO_6$ was measured in the vicinity of the magnetic transition temperature in the MPMS. An ac field was applied to an amount of the crystals (8.2 mg) without magnetic shielding; the applied ac field was thus superimposed on the Earth's field of ∼300 mOe. The amplitude of the applied ac field ($H_{ac}$) was 0.1, 0.3, 1, and 3 Oe, and the fundamental frequency (*f*) was 10, 132, 500, and 1000 Hz.

The specific heat ($C_p$) of an amount of crystals (3.6 mg) was measured in a commercial instrument (Quantum Design PPMS) between 3 and 300 K, with and without an applied field of 50 kOe.

We tried to measure the electrical resistivity of a single crystal of $Ca_3LiOsO_6$; however, it was too high to measure correctly. The electrical resistance was greater than $0.2 \times 10^6$ Ω at room temperature.

The electronic structure of $Ca_3LiOsO_6$ was calculated within the generalized gradient approximation[57] of density functional theory. We used the WIEN2k program,[58] which is based on full-potential augmented plane-wave (APW) methods. The spin−orbit interaction is included as a perturbation to the scalar-relativistic equations. The

(56) Batchelder, D. N.; Simmonss, R. O. *J. Chem. Phys.* **1964**, *41*, 2324.

(57) Perdew, J. P.; Burke, K.; Ernzerhof, M. *Phys. Rev. Lett.* **1996**, *77*, 3865.

(58) Blaha, P.; Schwarz, K.; Madsen, G. K. H.; Kvasnicka, D.; Luitz, J. *WIEN2k, An Augmented Plane Wave + Local Orbitals Program for Calculating Crystal Properties*; Techn. Universität Wien: Vienna, Austria, 2001.

***Table 3.*** Bond Lengths (Å), Bond Valence Sums,[a] and Bond Angles (Deg) in $Ca_3LiOsO_6$

| bond | bond length/ BVS | bond/ angle | bond length/ bond angle |
|---|---|---|---|
| Os−O (×6) | 1.9559(16) | Os−Ca (×6) | 3.1305(3) |
| BVS (Os) | 4.73 | Os−Li (×2) | 2.6950(1) |
| | | | |
| Li−O (×6) | 2.440(4) | Os−O−Li | 80.02(6) |
| BVS (Li) | 0.77 | O−Os−O (×6) | 89.46(7) |
| | | O−Os−O (×6) | 90.54(7) |
| Ca−O (×2) | 2.3236(17) | O−Os−O (×3) | 180 |
| Ca−O (×2) | 2.4762(18) | O−Li−O (×6) | 76.49(6) |
| Ca−O (×2) | 2.4848(17) | O−Li−O (×3) | 89.90(8) |
| Ca−O (×2) | 2.7430(18) | O−Li−O (×3) | 127.71(9) |
| BVS (Ca) | 2.01 | O−Li−O (×3) | 149.02(9) |

[a] BVS $= \sum v_i$, $v_i = \exp[(R_0 - l_i)/B]$, $B = 0.37$, $R_0(Li^+) = 1.466$, $R_0(Ca^{2+}) = 1.967$, and $R_0(Os^{5+}) = 1.868$.[54]

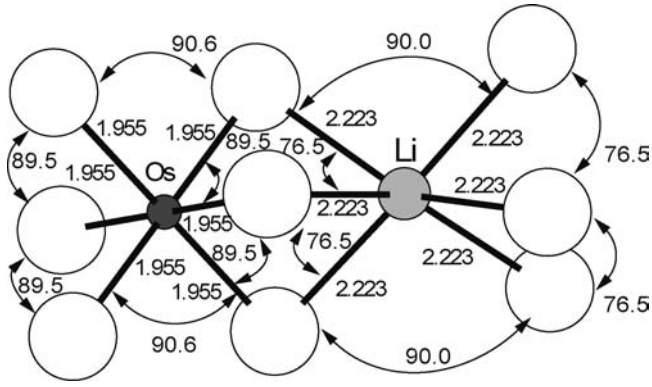


***Figure 2.*** Coordination environments of Os and Li atoms in $Ca_3LiOsO_6$. The numbers indicate the bond distances (Å) and the bond angles (°).

cutoff wave vector **K** for APW basis sets was chosen as $R\mathbf{K} = 8$, where $R$ is smallest muffin-tin radius, i.e., 1.7 au, for oxygen atoms. Integration over the Brillouin zone was approximated by a tetrahedron method with 110 $k$-points in an irreducible zone.

## 3. Results

Crystal structure at room temperature was successfully determined by the single-crystal X-ray method. Even though we did not use an initial model, the solution indicated that the trigonal ($R\bar{3}c$) model is highly reasonable, as often observed for $K_4CdCl_6$-type oxides. The $R$ factors decreased to a reliable level, 2.18% ($R_1$) and 5.90% (w$R_2$). In the analysis, we assumed that all sites for metal and oxygen atoms are fully occupied. We tested the assumption by investigating the thermal displacement parameters and bond valence sums (BVSs).[59,60] The thermal parameters are neither unusually small nor large, and BVS is not far from the expectation; thus, the assumption is not far from the truth. Although a relatively large Fourier residue, +4.93 e/Å$^3$, was observed, it remains within a normal level because the residue is usually smaller than approximately (atomic number)/10 e/Å$^3$ at a 0.6−1.2 Å distance for a reasonable structural model. Hence, the present value for Os (atomic number 76), at 0.61 Å, is unnoticeable. The final solutions are summarized in Table 2, and the calculated bond lengths, bond angles, and BVSs are listed in Table 3.

Figure 1c,d shows structural sketches drawn from the refined solution. As reported for the $K_4CdCl_6$-type oxides, it looks

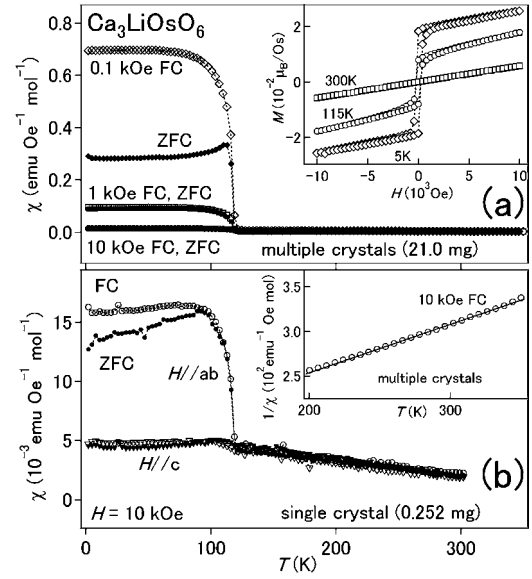


***Figure 3.*** (a) Temperature dependence of the magnetic susceptibility of single crystals (21.0 mg) of $Ca_3LiOsO_6$ oriented randomly in applied fields of 0.1, 1, and 10 kOe. The inset shows the field dependence of the isothermal magnetization at 5, 115, and 300 K. (b) Temperature dependence of the magnetic susceptibility of single crystals (0.252 mg) of $Ca_3LiOsO_6$ oriented parallel (**H**||$c$) and perpendicular (**H**||$ab$) with respect to the applied field of 10 kOe. The inset shows an inverse plot of the magnetic susceptibility data (10 kOe) for the multiple single crystals. The solid line corresponds to the fit.

structurally anisotropic toward 1D. The chain, however, contains not only the magnetic $OsO_6$ octahedra but also the nonmagnetic $LiO_6$ trigonal prisms, connected by sharing those faces alternately along the $c$-axis (see Figure 1d). Because the Li atom is incapable of mediating magnetic correlations between d electrons of Os atoms according to the first-principles calculation (shown later) and the nearest-neighbor Os atoms are rather distant (5.39 Å in the intrachain and 5.65 Å in the interchain), the magnetic interaction is expected to be rather feeble, regardless of the structural anisotropy.

Figure 2 shows the local coordination of Os and Li determined by the structure analysis. The atom $Os^{5+}$ ($5d^3$) is coordinated by six oxygens, forming the octahedral $OsO_6$; thus, the 5d state is split into $t_{2g}$ and $e_g$ states due to the relatively large crystal field of 10 Dq. Additionally, the octahedral $OsO_6$ does not have notable distortions, suggesting that the $t_{2g}$ band is nearly half filled ($S = 3/2$).[8,9] The $t_{2g}^3$ configuration suggests that the spin−orbital (SO) coupling is fairly weak, even in the strong SO coupling limit, since orbital angular momentum vanishes effectively ($L_{eff} = 0$). Thus, $S$ is expected to be a good quantum member of $Ca_3LiOsO_6$, unlike for the related 5d oxide $Sr_2IrO_4$, which has effective orbital and total magnetic momentum $L_{eff} = 1$ and $J_{eff} = 1/2$.[61,62]

Figure 3a shows the magnetic properties of multiple crystals of $Ca_3LiOsO_6$ loosely gathered in a sample holder. It is notable that the magnetic susceptibility increases steeply at ∼120 K on cooling, suggesting establishment of a long-range magnetic order. To study this further, isothermal magnetization was measured in the vicinity of and below and above the transition

(59) Brown, I. D. *Acta Crystallogr. B* **1977**, *33*, 1305.
(60) Yamaura, J.; Yonezawa, S.; Muraoka, Y.; Hiroi, Z. *J. Solid State Chem.* **2006**, *179*, 336.
(61) Kim, B. J.; Jin, H.; Moon, S. J.; Kim, J.-Y.; Park, B.-G.; Leem, C. S.; Yu, J.; Noh, T. W.; Kim, C.; Oh, S.-J.; Park, J.-H.; Durairaj, V.; Cao, G.; Rotenberg, E. *Phys. Rev. Lett.* **2008**, *101*, 076402.
(62) Kim, B. J.; Ohsumi, H.; Komesu, T.; Sakai, S.; Morita, T.; Takagi, H.; Arima, T. *Science* **2009**, *323*, 1329.

temperature. Systematic evolution of the sharp, step-like magnetization curve was clearly observed, suggesting a soft magnetism, with a small spontaneous magnetization. The magnetization is smaller than 0.02 $\mu_B$/Os at 5 K, corresponding to only 0.7% of the expected magnetic moment of the fully ordered $S = 3/2$ FM state. The magnetic data thus suggest that $Ca_3LiOsO_6$ undergoes an AF transition at $T_N \approx 120$ K, accompanying the weak magnetization most likely due to a Dzyaloshinsky−Moriya interaction generated by the broken inversion symmetry.[63]

In order to further study the magnetism, we applied the Curie−Weiss law to analyze the paramagnetic part (>200 K), as shown in the inset to Figure 3b. The analytical formula was $\chi(T) = N_A\mu_{eff}^2/3\pi(T - \Theta_W)$, where $N_A$ is the Avogadro constant and $\Theta_W$ is the Weiss temperature. The effective Bohr magneton ($\mu_{eff}$) was estimated to be 3.81(1) $\mu_B$, being fairly close to the expected moment (3.87 $\mu_B$) for the localized $S = 3/2$ system, confirming the expected $t_{2g}^3$ state ($L_{eff} = 0$) for $Ca_3LiOsO_6$. For the double perovskite $La_2NaOsO_6$ that has the isolated $Os^{5+}$ in the octahedral environment, 3.87 $\mu_B$ was found,[64] comparable with the present result. The $\Theta_W$ was −260(4) K, suggesting AF correlations are dominant in the spin system. Besides, the result leads to $|\Theta_W/T_N| \approx 2.2$, implying that magnetic frustration is very weak, in contrast to what was observed for the other $K_4CdCl_6$-type oxides.[20,32]

Figure 3b shows the crystal direction dependence of $\chi$. A single crystal of $Ca_3LiOsO_6$ was used in the measurements instead of multiple crystals. The crystal was set in a holder to have the chain-direction (*c*-axis) parallel or perpendicular to the applied field (10 kOe). The sample holder contribution was carefully subtracted from the raw data. It is obvious that the $\mathbf{H}\|ab$ curve goes beyond the $\mathbf{H}\|c$ curve, while the difference is insignificant above $T_N$. Thus, it is clear that the magnetic anisotropy is caused by AF ordering; however, the degree of the magnetic anisotropy is fairly small, ~3 ($\chi_{\mathbf{H}\|ab}/\chi_{\mathbf{H}\|c}$ at 5 K), which is much smaller than for the other chain compounds.[65] The single-crystal magnetic data imply that the ordered moments are weakly collinear to the *c*-axis.

The magnetic features were further studied by measurements of ac-$\chi$ in the vicinity of the magnetic transition temperature. The data are shown in Figure 4. At the magnetic transition point, a sharp peak was clearly observed in both the real (Figure 4a) and the imaginary (Figure 4b) parts, suggesting that the AF transition is likely a thermodynamic transition, in contrast to what was observed for a related compound.[27] However, a small degree of peak shift is observed toward the high-temperature side upon increasing the frequency of $H_{ac}$, suggesting a magnetically glassy nature somewhat involved in the spin system, probably caused by competition between many probably magnetite interactions, as will be discussed later. A detailed analysis of the frequency dependence is left for future study. It should be noted that the AF transition temperature is determined to be 117.0 K by the peak top position of the imaginary part at the lowest frequency. In addition, we also studied the magnitude of the $H_{ac}$ dependence of the peaks (Figure 4c,d). For clarification, the peaks in the real and the imaginary parts were normalized in intensity (shown in the inset to Figure 4c,d, respectively), confirming no visible shift.

(63) Moriya, T. *Phys. Rev.* **1960**, *120*, 91.
(64) Gemmill, W. R.; Smith, M. D.; Prozorov, R.; zur Loye, H.-C. *Inorg. Chem.* **2005**, *44*, 2639.
(65) Stitzer, K. E.; Abed, A. E.; Darriet, J.; zur Loye, H.-C. *J. Am. Chem. Soc.* **2001**, *123*, 8790.

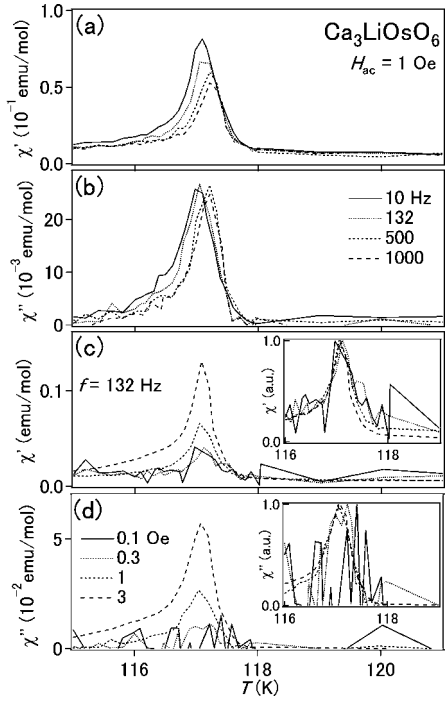


***Figure 4.*** Temperature and frequency (a,b) and applied field dependence (c,d) of the ac magnetic susceptibility ($\chi = \chi' + i\chi''$) of 8.2 mg of single crystals of $Ca_3LiOsO_6$. The insets in (c,d) show intensity-normalized data.

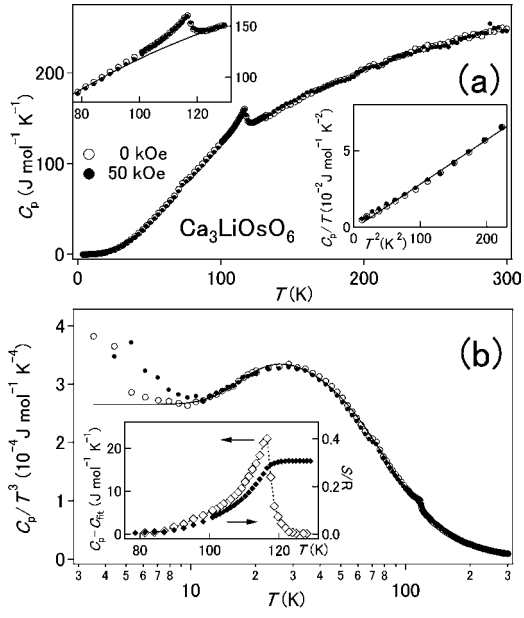


***Figure 5.*** (a) Temperature dependence of the specific heat of multiple crystals (3.6 mg) of $Ca_3LiOsO_6$ measured with and without the applied magnetic field of 50 kOe. The upper left inset indicates an expansion of the data in the vicinity of the peak. The lower right inset indicates the lowest temperature limit of the data in the plot of $C_p/T$ vs $T^2$. (b) Plot of the data for $C_p/T^3$ vs $T$. The inset shows $C_p - C_{fit}$ and entropy change in the vicinity of the magnetic transition temperature. Solid line and curves correspond to the fit.

Figure 5a shows the temperature and magnetic field dependence of $C_p$ of $Ca_3LiOsO_6$ between 2 and 300 K. Multiple crystals (total amount 3.6 mg) were fixed by a small amount of grease on a sample stage. The grease contribution to the $C_p$ data was subtracted from the raw data. The data shown in Figure 5a clearly indicate a notable peak in the vicinity of $T_N$, reflecting

that the magnetic transition is of a bulk nature. The peak part was roughly separated from the body of the $C_p$ data by applying a polynomial function, as shown in the inset to Figure 5a (upper left), allowing us to estimate the entropy change to be $\sim 0.31R$ ($R$ is the ideal gas constant). This corresponds to only 22% of the expected change ($\ln 4R$) for the ideal $S = 3/2$ system. It is likely that much of the entropy is removed via short-range ordering above $T_N$.

We analyzed the low-temperature part of $C_p$ (<15 K) by using the approximate Debye model, $C(T)/T = \beta T^2 + \gamma$, where $\beta$ is a coefficient and $\gamma$ is the Sommerfeld coefficient. Consistent with the model, the $C_p/T$ vs $T^2$ plot indeed shows a line feature (see the inset to Figure 5a) far below $T_D$ (the Debye temperature). Fitting to the linear part yielded $\beta = 2.91(5) \times 10^{-4}$ J mol$^{-1}$ K$^{-4}$ and $\gamma = 0.00(1)$ mJ mol$^{-1}$ K$^{-2}$. We obtained $T_D = 419(2)$ K from this $\beta$. The $C_p$ data measured in a magnetic field of 50 kOe were analyzed as well, yielding $\beta = 2.85(5) \times 10^{-4}$ J mol$^{-1}$ K$^{-4}$ and $\gamma = 0.00(1)$ mJ mol$^{-1}$ K$^{-2}$; thus, $T_D = 422(3)$ K. The difference between the two sets of parameters is insignificant, suggesting the absence of additional magnetic contributions at the low temperature limit.

The entire $C_p$ was quantitatively analyzed by a linear combination of the Debye model and the Einstein model, as it successfully fits the $C_p$ data of several osmium oxides.[66] The data are plotted in the lattice specific heat, $C_p/T^3$ vs $T$, in Figure 5b. The analytical formula was

$$C(T) = n_D 9 N_A k_B \left(\frac{T}{T_D}\right)^3 \int_0^{T_D/T} \frac{x^4 e^x}{(e^x - 1)^2} dx + n_E 3 N_A k_B \left(\frac{T_E}{T}\right)^2 \frac{e^{T_E/T}}{(e^{T_E/T} - 1)^2}$$

where $N_A$ is Avogadro's constant, $k_B$ is the Boltzmann constant, and $T_E$ is the Einstein temperature. The scale factors $n_D$ and $n_E$ correspond to the number of vibrating modes per formula unit in the Debye and Einstein models, respectively. Fit to the data yielded $T_D = 413(1)$ K, $T_E = 130(1)$ K, $n_D = 9.61(7)$, and $n_E = 0.285(9)$. The Einstein contribution appears as a broad hump in the lattice plot. The small Einstein term possibly suggests that anharmonic lattice dynamics exist somewhat in $Ca_3LiOsO_6$, as discussed for the pyrochlore osmium oxides.[66] To further investigate the lattice dynamics, $C_p$ in the magnetic field of 50 kOe was analyzed as well: the fit yielded $T_D = 414(2)$ K, $T_E = 125(1)$ K, $n_D = 9.62(8)$, and $n_E = 0.246(11)$, indicating little change. Additional studies are needed to clarify the origin of the hump in the lattice specific heat of $Ca_3LiOsO_6$.

In the specific heat measurements, we observed a sharp peak corresponding to the AF transition. However, it shows little change in the 50 kOe field, suggesting that a nonmagnetic transition might accompany the AF transition. We thus conducted a low-temperature XRD study on $Ca_3LiOsO_6$ to test a possible structure change at $T_N$. The XRD patterns are shown in Figure 6a in the order of the temperature where the measurement was taken. We observed only a monotonic change over $T_N$; such as a peak split and the appearance/disappearance of small peaks, corresponding to superstructure formation, were not detected above the XRD background, rejecting the possibility of a major structure change at $T_N$.

The change in lattice parameters was carefully deduced from the XRD patterns. Figure 6b−d shows the thermal evolution of the lattice parameters $a$ and $c$ and the volume $V$ of the trigonal unit cell, respectively. Above $T_N$, $a$, $c$, and $V$ all change monotonically; however, an anisotropic change occurs at $T_N$. The parameter $a$ decreases continuously over $T_N$, while $c$ stops decreasing at $T_N$ upon cooling. This suggests a possible coupling between the AF transition and the anisotropic structural change. Considering the ordered spins collinear to the $c$-axis, 5d orbital ordering may account for the possible coupling; otherwise, AF magnetostriction, as found for NiO and CoO,[67] may be responsible for the lattice anomaly. To shed more light on the issue, low-temperature neutron studies would be helpful.

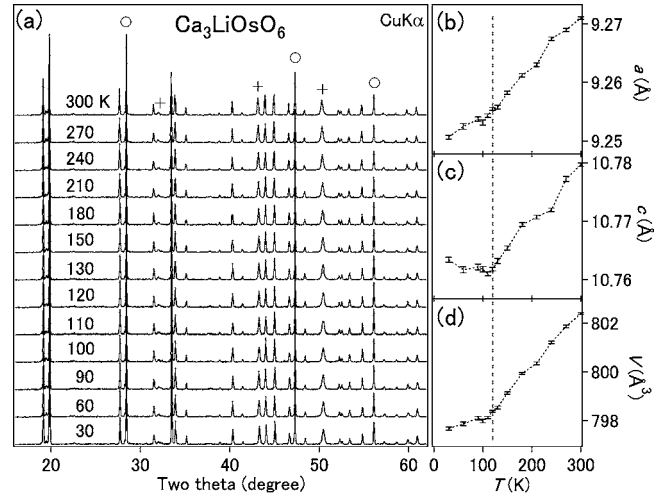


***Figure 6.*** (a) XRD patterns for the polycrystalline $Ca_3LiOsO_6$ measured at a fixed temperature between 30 and 300 K. Circles indicate peaks from Si standard mixed in the sample powder. Crosses indicate peaks from the sample stage. The thermal evolution of the lattice parameters of (b) $a$, (c) $c$, and (d) the trigonal unit-cell volume, $V$, of $Ca_3LiOsO_6$ is deduced from the XRD profiles. The broken line corresponds to the magnetic transition temperature.

## 4. Discussion and Conclusions

Regarding 3d oxides, SO coupling often has little effect on the total magnetism. However, the situation is different for 5d oxides, for which the SO coupling is approximately an order of magnitude greater than that of a 3d oxide. It is thus highly important to measure the contribution of the SO coupling in order to understand the 5d magnetism correctly. Indeed, the SO coupling plays a major role in the magnetism of the 5d oxide $Sr_2IrO_4$.[61,62] In $Ca_3LiOsO_6$, every $Os^{5+}$ $5d^3$ is octahedrally coordinated by oxygen; thus, the $t_{2g}^3$ configuration ($5d_{xy}^1\, 5d_{yz}^1\, 5d_{zx}^1$) is expected, indicating a nearly half-filled spin state ($S = 3/2$). It is notable that the observed magnetic moment of 3.81(1) $\mu_B$ matches 99% with the expected spin moment, indicating that the SO coupling contribution is indeed small. At the strong limit of the SO coupling, the $t_{2g}^3$ state has $L = 0$; thus, the agreement seems to be reasonable.

For comparison, we looked at the magnetic properties of the analogous 4d oxides having the $t_{2g}^3$ configuration. We found that the observed magnetic moments of $Sr_3LiRuO_6$, $Sr_3NaRuO_6$, $Ca_3NaRuO_6$, and $Ca_3LiRuO_6$ range between 78% and 87% of the expected spin moment for $S = 3/2$,[34] not far from the result for $Ca_3LiOsO_6$. This confirms that the $t_{2g}^3$ Ru oxides have little SO coupling contribution to the total magnetism, as for the Os oxide. We also tried to survey the magnetic properties of analogous 3d oxides such as $A_3A'FeO_6$ (A = Sr and Ca; A′ =

(66) Bruhwiler, M.; Kazakov, S. M.; Zhigadlo, N. D.; Karpinski, J.; Batlogg, B. *Phys. Rev. B* **2004**, *70*, 020503R.

(67) Nakamichi, T.; Yamamoto, M. *J. Phys. Soc. Jpn.* **1961**, *16*, 126.

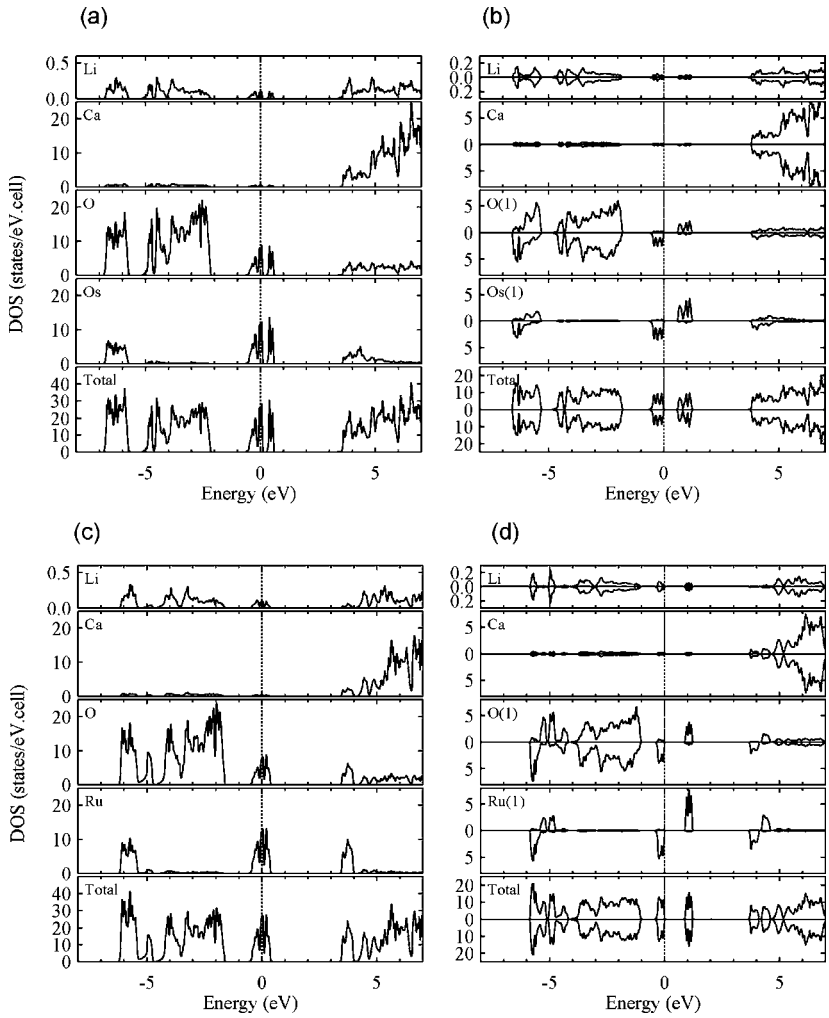


***Figure 7.*** Nonmagnetic (a,c) and antiferromagnetic (b,d) DOS of $Ca_3LiOsO_6$ (a,b) and $Ca_3LiRuO_6$ (c,d). The energy of the highest occupied state is set to zero. For the AF cases, the upper and lower panels show partial DOS for up and down spins, respectively. While the Os and O sites in the AF phase split into two inequivalent sites labeled by (1) and (2), only Os(1) and O(1) are shown for clarity. The partial DOS for Os(2) and O(2) may be generated by interchanging the spin up and down partial DOS for Os(1) and O(1), respectively.

Li and Na); however, it seems such compounds have not been synthesized to date, unfortunately.

We calculated the electronic structures of $Ca_3LiOsO_6$ from a first-principles method. The total and partial densities of states (DOS) for the nonmagnetic calculation are shown in Figure 7a for $Ca_3LiOsO_6$. When spin-polarization is ignored, they indicate a metal with the Fermi energy in $t_{2g}$ bands, ranging from $-0.6$ to 0.6 eV. These states are derived from antibonding combination between the $t_{2g}$ orbital of Os atoms and the $p_\pi$ orbital of neighboring oxygen atoms, while the bonding counterparts are distributed around $-7$ to $-5$ eV. The $e_g$ states of Os are distributed far above the Fermi level. The bandwidth of $t_{2g}$ bands is approximately 1.2 eV, narrower than for other typical Os oxides. For example, the $t_{2g}$ bandwidth of the perovskite oxide $NaOsO_3$ is larger than 3 eV.[8] The smaller bandwidth is a direct consequence of the local structure around Os atoms.

When magnetic ordering is taken into account, we obtained a stable AF solution, which has lower energy than the nonmagnetic one by $-0.6$ eV per Os atom. Magnetic moments are mostly distributed on Os atoms with $\pm 1.4\,\mu_B$ per atom. From hybridization between Os d and O p orbitals, O atoms contribute small magnetic moments of $\pm 0.1\,\mu_B$ per atom, which are parallel to that on the nearest Os atom. The calculated total and partial DOS for the AF solution are shown in Figure 7b. We found that the $t_{2g}$ bands are completely spin-polarized and the compound is calculated to be an insulator. The completely spin-polarized $t_{2g}$ bands are consistent with the experimental observation. We also performed first-principles calculations for the analogous 4d oxide $Ca_3LiRuO_6$, which shows a comparable magnetic nature. The results are shown in Figure 7c,d, indicating indeed a qualitatively comparable electronic structure.

Although the coulomb interaction is expected to be weak due to the nature of the 5d orbital, the narrow $t_{2g}$ bands suggest that correlation effects are important for $Ca_3LiOsO_6$. Therefore, from the calculated electronic structure and experimental observation, this compound can be considered as a 5d Mott insulator.[68,69] To date, only a few 5d oxides show Mott insulating behaviors; hence, it is of high interest to investigate the electronic state of $Ca_3LiOsO_6$ by such methods as angular-resolved photoemission spectroscopy and resonant X-ray scattering. Unlike what was suggested for $Sr_2IrO_4$, the SO coupling contribution should be little in the Mott insulating state of $Ca_3LiOsO_6$.

We would like to discuss the magnetic interactions responsible for the 117 K AF order in $Ca_3LiOsO_6$. The magnetic ordering temperature is remarkably high, 117 K, although the

(68) Mott, N. F. *Proc. Phys. Soc., London, Sect. A* **1949**, *62*, 416.
(69) Hubbard, J. *Proc. R. Soc. London, Ser. A* **1963**, *276*, 238.

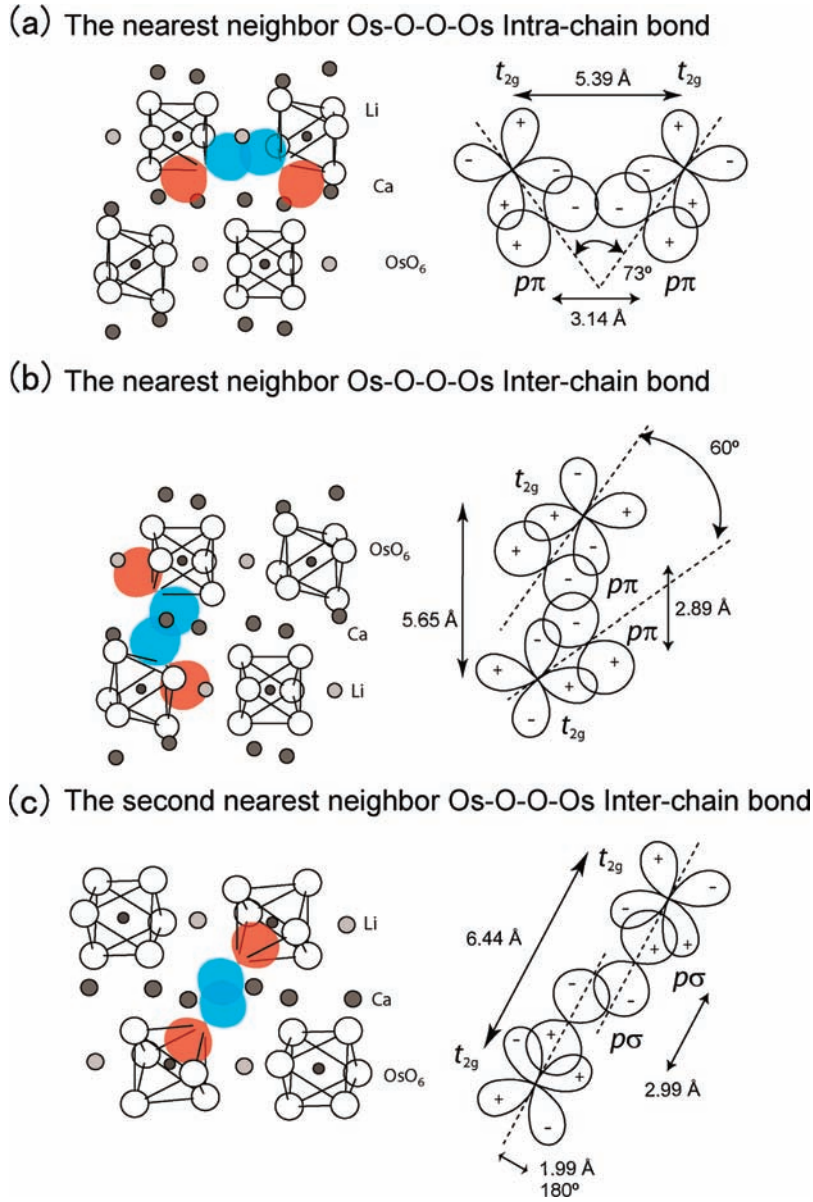


***Figure 8.*** Selected possible superexchange magnetic paths through two oxygen atoms in $Ca_3LiOsO_6$: (a) the nearest-neighbor intrachain bond $t_{2g}^3-p_\pi-p_\pi-t_{2g}^3$, (b) the nearest-neighbor interchain bond $t_{2g}^3-p_\pi-p_\pi-t_{2g}^3$, and (c) the next-nearest-neighbor 180° interchain bond $t_{2g}^3-p_\sigma-p_\sigma-t_{2g}^3$.

magnetic system has no original superexchange interaction path such as Os−O−Os. The distance between the nearest-neighbor Os atoms is 5.39 Å in the intrachain and 5.65 Å in the interchain, too far to establish the direct spin−spin interactions. Thus, we need to consider a possible extension of the superexchange magnetic interaction, which is capable of correlating spins through multiple nonmagnetic anions, as was discussed by Mizuno and Whangbo.[4−7] Figure 8 shows the nearest-neighbor (Os−O)−(O−Os) intrachain and interchain bonding and the next-nearest-neighbor interchain bonding in $Ca_3LiOsO_6$. The possible magnetic $p_\pi-p_\pi$ intrachain bonding (Figure 8a) is at an angle of 73° and a distance of 3.14 Å, while the $p_\pi-p_\pi$ interchain bond (Figure 8b) is connected at an angle of 60° and a distance of 2.89 Å. In the bonds, electron transfer or partial covalence may take place to some extent between neighboring d orbitals through two 2p orbitals. Additionally, the possible bonds $p_\pi-p_\sigma$ and $p_\sigma-p_\sigma$ (not shown for clarity) and the next-nearest-neighbor bond (Figure 8c) should contribute somewhat to the magnetic correlations. Although it is difficult to estimate the possible sign and intensity for every magnetic bond, it is likely that the sum of the possible magnetic bonds is responsible for the 117 K AF order.

From the viewpoint of Mott insulators, Anderson has formulated the superexchange interaction using orthogonal localized orbitals (Wannier orbitals).[70] This generalized theory may be applicable to spatially separated orbitals. According to this theory, the AF exchange coupling $J$ is described as $\sim t^2/U$, where $t$ is the hopping matrix element between neighboring localized orbitals and $U$ is the Coulomb integral for a localized orbital. For $Ca_3LiOsO_6$, localized Wannier orbitals corresponding to $t_{2g}$ bands would have moderate weights on the $p_\pi$ at adjacent oxygen atoms. This picture is supported by the calculated distribution of magnetic moments, as the oxygen atoms in an $OsO_6$ octahedron have magnetic moments parallel to that of the central Os atom. We may roughly estimate hopping $t$ as $W/2z$, where $W$ is the bandwidth and $z$ is the number of

(70) Anderson, P. W. *Phys. Rev.* **1959**, *115*, 2.

nearest-neighbor sites around a local orbital. For the present case, $t$ is estimated to be ~0.1 eV from $W \approx 1.5$ eV and $z = 8$. If $U$ is assumed to be 1−2 eV, $J$ may be estimated to be a reasonable value. Further quantitative theoretical consideration of the newly synthesized 5d oxide $Ca_3LiOsO_6$ as well as the 4d oxide $Ca_3LiRuO_6$ may help to judge the possible model of magnetic interaction through multiple oxygen atoms.

We considered the possibility that a trigonal ligand field splits the $t_{2g}$ triplet into an $a_{1g}$ singlet and an $e_g$ doublet in $Ca_3LiOsO_6$. The orbitals $a_{1g}$ and $e_g$ are equally occupied, and magnetic interaction is mainly from $a_{1g}$, which has a larger overlap with O atoms than $e_g$. We tested this possibility with a first-principles study; however we were unable to judge clearly the splitting picture. In order to practically test the possibility, it may be helpful to study "$Ca_3LiRhO_6$" or "$Ca_3LiIrO_6$", if those are available, because $a_{1g}$ accommodates two paired electrons, resulting in the electronic configuration for $Rh^{5+}(Ir^{5+})$ $a_{1g}{}^2$ $e_g{}^2$, $S = 1$. In this configuration, magnetic correlations between the neighboring $TrO_6$ octahedra may be terminated because there are no states available for the electron transfer responsible for the magnetic correlation. The compounds "$Ca_3LiRhO_6$" and "$Ca_3LiIrO_6$" are thus expected to be magnetically different in nature from "$Ca_3LiRuO_6$" and "$Ca_3LiOsO_6$" if the splitting picture is reasonable. Additional studies toward the synthesis of "$Ca_3LiRhO_6$" and "$Ca_3LiIrO_6$" are in progress.

In summary, we synthesized the osmium oxide $Ca_3LiOsO_6$ for the first time and successfully obtained single crystals having ~0.6 mm size in the largest dimension. The crystal is highly resistive electrically, and its measured $\gamma$ is practically zero, indicating that the electronic gap is fully opened. $Ca_3LiOsO_6$ is thus highly expected to be a Mott insulator, despite $U$ being much smaller than that of 3d oxides. First-principles calculation indicated that the 5d bandwidth is indeed narrow, reflecting the distant nature of the $OsO_6$ arrangement. The small $W$ is probably sufficient to open the gap in $Ca_3LiOsO_6$. In addition, we found that the magnetic ground state is AF and the long-range order is established at the remarkably high temperature of 117 K (comparable with the so-far highest recorded for $K_4CdCl_6$-type magnetic oxides). Because the original superexchange magnetic interaction through Os−O−Os is negligibly small in $Ca_3LiOsO_6$, the observed order is likely due to the extended magnetic path (Os−O)−(O−Os). If this is true, the newly synthesized $Ca_3LiOsO_6$ is valuable, along with $Ca_3LiRuO_6$, for further studies of the extended superexchange magnetic interaction in solids.

**Acknowledgment.** We thank Dr. S. Okamoto (ORNL) for valuable discussions. This research was supported in part by "WPI Initiative on Materials Nanoarchitectonics" from the Ministry of Education, Culture, Sports, Science and Technology, Japan; "Research Seeds Quest Program", managed by the Japan Science and Technology Agency; and "Grants-in-Aid for Scientific Research (20360012, 22246083)" and "Funding Program for World-Leading Innovative R&D on Science and Technology (FIRST Program)", managed by the Japan Society for the Promotion of Science.

**Supporting Information Available:** Crystallographic information file for $Ca_3LiOsO_6$. This material is available free of charge via the Internet at http://pubs.acs.org.

JA102606Q